Environmental Research Communications

OPEN ACCESS

RECEIVED
18 July 2025

REVISED
22 October 2025

ACCEPTED FOR PUBLICATION
31 October 2025

PUBLISHED
13 November 2025

LETTER

Intensifying intraseasonal oscillation of South China Sea winter upper-layer circulation in a warming climate

Jingyao Cai[1,4], **Mingkui Li**[1,2,4], **Jinzhuo Cai**[1,*], **Xin Ma**[1,2,*], **Haiyuan Yang**[1,2], **Xingzhi Zhang**[1,3], **Jingjie Yu**[1] **and Zhaohui Chen**[1,2]

[1] Frontier Science Center for Deep Ocean Multispheres and Earth System (FDOMES)/Academy of the Future Ocean and Physical Oceanography Laboratory, Ocean University of China, Qingdao, People's Republic of China
[2] Laboratory for Ocean Dynamics and Climate, Qingdao Marine Science and Technology Center, Qingdao, People's Republic of China
[3] Laoshan Laboratory, Qingdao, People's Republic of China
[4] These authors contributed equally: Jingyao Cai and Mingkui Li.
[*] Authors to whom any correspondence should be addressed.

E-mail: cjz@stu.ouc.edu.cn **and** maxin@ouc.edu.cn

Keywords: global warming, South China Sea circulation, intraseasonal oscillation, ocean stratification

Supplementary material for this article is available online

Abstract

The upper-layer circulation in the South China Sea (SCS) exhibits significant intraseasonal oscillation (ISO), influencing the regional ocean environment and climate. However, the evolution of this ISO under global warming and its underlying mechanisms remain poorly understood. Using a high-resolution Community Earth System Model, this study identifies a strengthening trend of 7.8% in the ISO intensity of the western boundary current (WBC) speed during 1901–2100. Further analysis reveals a 24% intensification of oceanic stratification, while basin-scale wind stress and its ISO show weakening trends of 10% and 18%, respectively. Quasi-geostrophic model experiments demonstrate that the ISO enhancement is primarily driven by intensified upper-ocean stratification, with the weakening wind field exerting a dampening effect. This amplified upper-layer circulation ISO is closely linked to increased sea surface temperature (SST) variability, suggesting higher intensity and frequency of marine heatwaves in the SCS. Furthermore, enhanced SST variability may amplify intraseasonal ocean heat release, potentially altering regional climate. This study elucidates the intensification mechanism of upper-ocean ISO in the SCS under global warming and its climatic impacts, providing new insights into the response of tropical marginal sea climate variability to a warming climate.

1. Introduction

The South China Sea (SCS) Basin is a semi-enclosed marginal sea of profound scientific significance (Lan *et al* 2006). Driven by the seasonally varying East Asian Monsoon, the upper-layer circulation of the SCS exhibits a double-gyre pattern in summer and a basin-scale cyclonic pattern in winter (Xu *et al* 1982, Fang *et al* 2002, Wang *et al* 2006, Shaw and Fu 1999, Li and Qu 1999). Owing to the stronger wind forcing in winter compared to summer, the annually averaged wind field exhibits winter-monsoon-dominant characteristics. From October to April of the following year, the strong southwestward wind stress can reach 0.3 $N{\cdot}m^{-2}$ (Chu *et al* 1999, Lan *et al* 2006), leading to a basin-wide positive wind stress curl across the SCS (Yang *et al* 2017). Following a 1–3 months adjustment associated with the first-order baroclinic Rossby waves, the upper-layer circulation reaches quasi-steady Sverdrup balance, forming the strong western boundary current (WBC) along the Vietnamese coast. The WBC flows southward with speed exceeding 0.5 $m{\cdot}s^{-1}$ and volume transport of 7 Sverdrup ($1\ Sv = 1 \times 10^6\ m^3{\cdot}s^{-1}$), transporting cold water from the northern SCS, contributing to the formation of a prominent cold tongue in the southern basin (Fang *et al* 2012, Meng *et al* 2024).

In addition to the seasonal cycle of the upper-layer circulation, the intraseasonal oscillation (ISO) represents a dominant signal across the tropical Indian Ocean, the SCS, and the tropical western North Pacific regions (Cao *et al* 2017). In the SCS, surface currents exhibit robust 30–60-day ISO, with speed anomalies exceeding 50% of the mean flow (Zhou and Chan 2005, Yang *et al* 2017). It has been agreed that the energy contained in the intraseasonal scale ocean dynamic process is far greater than that of interannual and interdecadal, closely relating to the energy dissipation of the ocean (Qiu and Chen 2005, Ferrari and Wunsch 2009). Due to the significant upwelling and abundant fishery ecological resources along the Vietnamese coast, previous studies have found that the ISO of the current speed plays an important role in the nearshore fishing grounds, primary productivity pulses and the oscillation of the offshore current, which is also closely related to atmospheric oscillations (Wang *et al* 2013, Hu *et al* 2016). Studies indicate that the ISO, influenced by the tropical Madden-Julian Oscillation, induces significant variations in the SCS surface circulation, thereby modulating the intrinsic ISO of SCS (Hu *et al* 2024). Enhanced wind forcing intensifies surface circulation, increasing kinetic energy of water masses and amplifying instability, which generates more pronounced oscillations (Hu *et al* 2024). For example, mesoscale eddies from current instabilities along the Vietnamese coast (Gan and Qu 2008) and baroclinically unstable winter circulations (Wang *et al* 2020) modulate ISO energy through Rossby wave adjustment (Zhuang *et al* 2010).

Since the onset of the Industrial Revolution in the mid-19th century, the global climate system has experienced substantial warming, with the oceans absorbing approximately 90% of the excess heat (von Schuckmann *et al* 2020), resulting in pronounced upper-ocean warming, enhanced global ocean stratification (Li *et al* 2020), and more frequent marine heatwaves (Cai and Tan 2024). These thermal and dynamical changes have significantly modulated the vertical structure of ocean circulation (Peng *et al* 2022, Yang *et al* 2025), leading to enhanced upper-layer mean flow and oscillation accompanied by a more quiescent deep ocean (Wang *et al* 2024). Because the surface-layer circulation is largely driven by the relative potential vorticity, and the thickness potential vorticity (TPV) plays a damping role, the effect of TPV is weakened and the surface circulation becomes stronger with ehanced stratification (figure S4; Pedlosky 1987, Sun *et al* 2013, Yao *et al* 2017, Peng *et al* 2022, Zhu *et al* 2024, Yang *et al* 2025). This process enhances the horizontal shear of the WBC, giving the current more barotropic instability, and leading to increased generation of mesoscale activities with a period of 20–90 days in the off-shore region of winter WBC (figure S5; Liu 1997, Sun *et al* 2013, Lin *et al* 2015, Feng *et al* 2017). In comparison, the East Asian winter monsoon has concurrently exhibited a marked weakening trend since the 1970s (Wang and He 2012, Kang *et al* 2022, Cai and Tan 2024), directly reducing WBC intensity (Yang and Liu 1998). Dynamically, the ISO of ocean circulation is intrinsically linked to both the structural characteristics and intensity of the circulation system (Liu *et al* 2023), implying that global warming may influence ISO of ocean circulation through direct external forcing mechanisms such as wind variability and indirect effects mediated by changes in circulation intensity and ocean stratification. Nevertheless, the specific response of the ISO in the SCS to global warming remains poorly constrained, hindering a comprehensive understanding of the underlying dynamical processes.

To address the above issues, this paper uses long-term high-resolution model data to study the trend of the ISO of the upper-layer circulation in the SCS in winter, and to explore the relative importance of wind and stratification on the ISO change. This paper is organized as follows: section 2 briefly introduces the data and method. In section 3, a detailed study of the trend of ISO of ocean circulation and associated mechanisms is presented, followed by the potential implications of the change of ISO of ocean circulation in section 4. This paper ends with a summary in section 5.

2. Data and method

2.1. Data

2.1.1. Data from CESM model

To explore the trend of ISO of SCS upper-layer circulation, outputs from the high-resolution Community Earth System Model (CESM; Wan *et al* 2014) are used. The CESM is developed based on the coupled climate model framework from the National Center for Atmospheric Research's Climate and Global Dynamics Laboratory. This dataset features a high spatial resolution of $0.1^\circ \times 0.1^\circ$ and a high temporal resolution of 1 day. The CESM experiments are conducted within the framework of the Coupled Model Intercomparison Project Phase 5 (Taylor *et al* 2012). The oceanic component of CESM utilizes POP2 with 62 vertical layers and 3600×2400 horizontal grids for detailed ocean circulation dynamics. The atmospheric component uses CAM5.2 with 30 vertical layers with 2.25 hPa top pressure, and $0.25^\circ \times 0.25^\circ$ horizontal resolution for improved atmospheric circulation representation. The CESM's ocean module is spun up under fixed preindustrial (1850) climate conditions for 250-year from a quiescent ocean state (Chang *et al* 2020). During 1850–2005, historical forcings were utilized, whereas for the period after 2005, RCP8.5 forcing fields were employed. Previous research utilizing the CESM has conducted global warming studies covering the North Pacific, tropical Pacific, and other oceanic regions from 1850 to 2100, confirming a strong capability for

studying ocean variability under global warming (Shang *et al* 2023). Here, we focus on the domain covering the SCS (0°N–21°N, 100°E–120°E) during the winter (December to February) from 1901 to 2100.

2.1.2. Data from ECCO2

To examine the robustness of CESM outputs, reanalysis current data from the Estimating the Circulation and Climate of the Ocean, Phase II (ECCO2) is applied. The dataset employs an eddy-permitting grid with a spatial resolution of $0.25^\circ \times 0.25^\circ$, and incorporates a Green-function-based four-dimensional variational assimilation framework that ingests observed data from World Ocean Circulation Experiment, Argo and Tropical Atmosphere Ocean arrays together with satellite-derived products such as sea-level anomalies. Similar to the CESM data, the region (0°N–21°N, 100°E–120°E) is focused, while the time is the winter (December to February) from 1992 to 2018.

2.1.3. Data from Quasi-Geostrophic model

To elucidate the mechanisms governing the ISO of ocean circulation changes, we design numerical experiments based on a two-layer Quasi-Geostrophic (QG) ocean model. As a classical ocean dynamics tool, the QG model is widely used in studies in dynamic processes of ocean circulation (Yang *et al* 2015, Xu and Wang 2024). Following the previous studies (Sun *et al* 2013, Yang *et al* 2015), the SCS basin is simplified to a rectangular basin with zonal width (L_x) of 1000 km and meridional width (L_y) of 1800 km. The horizontal resolution of the QG model is 8 km, while the temporal step is 1 day. The governing equations for the two-layer QG model are as follows (equations (1), (2); Pedlosky 1987, Berloff *et al* 2007, Sun *et al* 2013):

$$\frac{\partial q_1}{\partial t} + J(\Psi_1, q_1) = \frac{f_0}{H_1} W + A_H \nabla^4 \Psi_1, \tag{1}$$

$$\frac{\partial q_2}{\partial t} + J(\Psi_2, q_2) = A_H \nabla^4 \Psi_2 - \gamma \nabla^2 \Psi_2. \tag{2}$$

These governing equations include potential vorticity (q_i), the stream function (ψ_i), layer thickness (H_i), dissipation term ($A_H \nabla^4 \Psi$), wind forcing (W), and viscous term ($\gamma \nabla^2 \Psi$), where i ($i = 1,2$) is the layer index starting from the top. Here, the symbol $J(a,b) = a_x b_y - a_y b_x$ is the Jacobian operator. The model adopts a β-plane approximation, with the Coriolis parameter $f_0 = 3.86 \times 10^{-5}\ \mathrm{s}^{-1}$ and its meridional gradient $\beta = 2.25 \times 10^{-11}\ \mathrm{m}^{-1}\cdot\mathrm{s}^{-1}$. $A_H = 140\ \mathrm{m}^2\cdot\mathrm{s}^{-1}$ is the horizontal eddy viscosity coefficient, and $\gamma = 10^{-7}\ \mathrm{m}\cdot\mathrm{s}^{-1}$ is the linear bottom friction coefficient (table S1). The potential vorticity q_1 and q_2 are defined as follows:

$$q_1 = \nabla^2 \psi_1 + F_1(\psi_2 - \psi_1) + \beta y, \tag{3}$$

$$q_2 = \nabla^2 \psi_2 + F_2(\psi_1 - \psi_2) + \beta y, \tag{4}$$

$$F_1 = \frac{f_0^2}{g' H_1},\ F_2 = \frac{f_0^2}{g' H_2}, \tag{5}$$

where $g' = g(\rho_2 - \rho_1)/\rho_0$ represents the reduced gravity, g is the gravitational constant, ρ_0 and ρ_i indicate the reference density and the density of layer i (values of g' is available at table S1). In addition, the model is driven by an idealized sinusoidal wind field (W) through Ekman pumping mechanism:

$$W = \tau_0 \sin\left(\frac{\pi y}{L_y}\right)[1 + k \sin(\omega t)]. \tag{6}$$

Here, τ_0 represents average Ekman pumping rate, k, ω regulate the amplitude and frequency of the ISO of Ekman pumping rate, respectively (table S1).

To distinguish the different role played by the surface wind and oceanic stratification in affecting the ISO of ocean circulation, four sets of idealized experiment are conducted by manipulating parameters related to the wind (τ_0, k) and stratification (H_1, H_2, g'). Each experiment is spun up for 1460 days from rest and the ISO of ocean circulation is calculated from the last 90 days. More settings will be introduced in section 3.3.

2.2. Method

Following previous studies, we employ standard deviation (STD) as the metric to quantify ISO intensity (Dong *et al* 2009, Yang *et al* 2017). Taking the current speed as an example, when calculating the intensity of ISO as in equation (7):

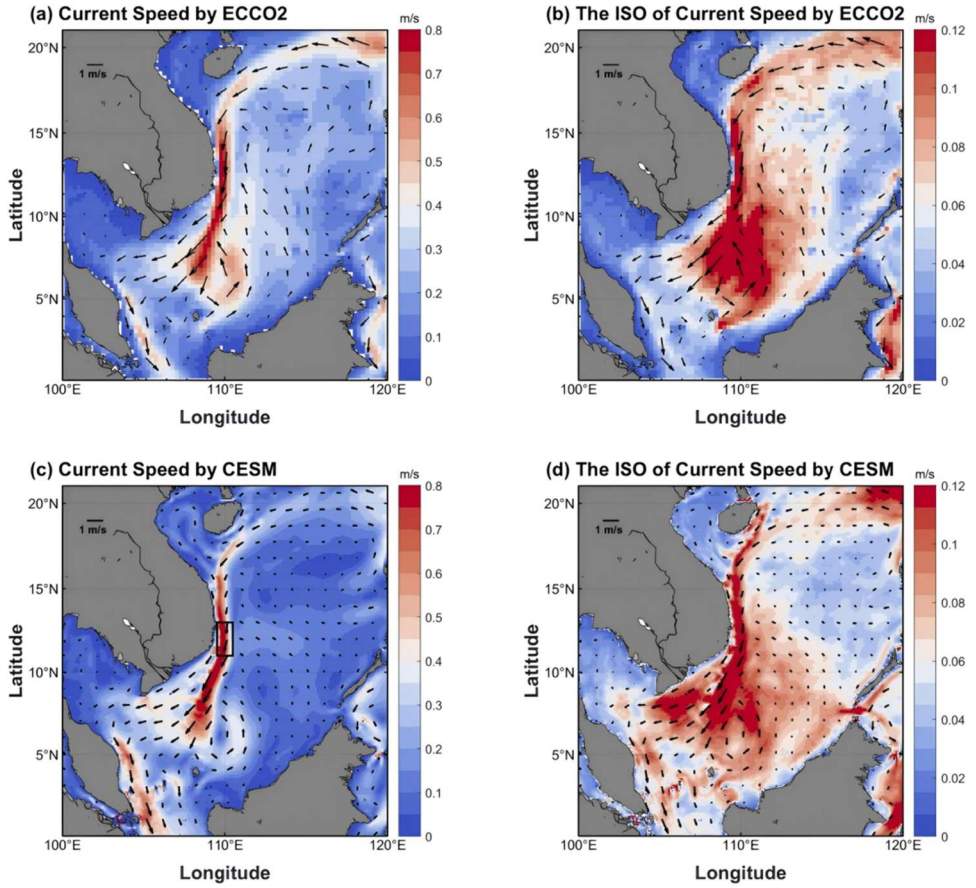

Figure 1. Comparison between ECCO2 and CESM data on winter current speed in the SCS from 1992 to 2018. (a) Mean ECCO2 current speed. (b) ISO of ECCO2 current speed. (c) Mean CESM current speed, similar to (a). (d) ISO of CESM current speed, similar to (b). The shading indicates the current speed, and arrows show the direction. The black rectangle in (c) is the region of calculating transport in section 3.3.

$$ISO\_cur = \sqrt{\frac{\sum(v_i - \mu)^2}{d}}. \tag{7}$$

The ISO of the current speed (*ISO_cur*) is calculated by taking the square root of the average squared deviation of daily current speed v_i from their mean μ over the days d in this year's winter, where i ($i = 1,2\ldots\ldots90$) represents the sequential winter day for each year. In order to eliminate the influence of seasonal cycle, we remove the linear trend from each 90-day winter window and perform a 20–60-day bandpass filtering before the ISO calculation. All the calculation of ISO of physical quantity in this paper is similar to the *ISO_cur*. To better isolate trends in ISO under global warming from the interannual signals such as the El Niño-Southern Oscillation (ENSO), a 4-year smoothing filter is applied to the timeseries of ISO before calculating their long-term trends. This approach ensures that the resulting trends are primarily attributed to global warming (Kelly and Jones 1996).

3. The intensifying ISO in upper-layer circulation under global warming

3.1. Data validation

Before exploring the *ISO_cur* change in SCS, it is necessary to quantify whether the CESM model can reasonably simulate the associated dynamical processes. Figures 1(a) and (c) show the sea surface speed obtained from ECCO2 and CESM model outputs. Reanalysis data indicate the wintertime WBC in the SCS has an average speed of approximately 0.38 m·s^{-1}, while the CESM simulation yields 0.28 m·s^{-1}, both consistent with previous studies (Wu *et al* 1998, Yang *et al* 2015). The simulated WBC's offshore point (~12°N) also aligns with reanalysis data and previous studies (figures 1(a), (c); Fang *et al* 2012). The *ISO_cur* of the winter WBC is well-captured by the model. The simulated *ISO_cur* in WBC region is 0.087 m·s^{-1}, matching the reanalysis data of ~0.094 m·s^{-1} (figures 1(b), (d)). These results demonstrate excellent agreement between CESM and ECCO2 in reproducing both the spatial patterns of multi-year mean current speed fields and the distribution of

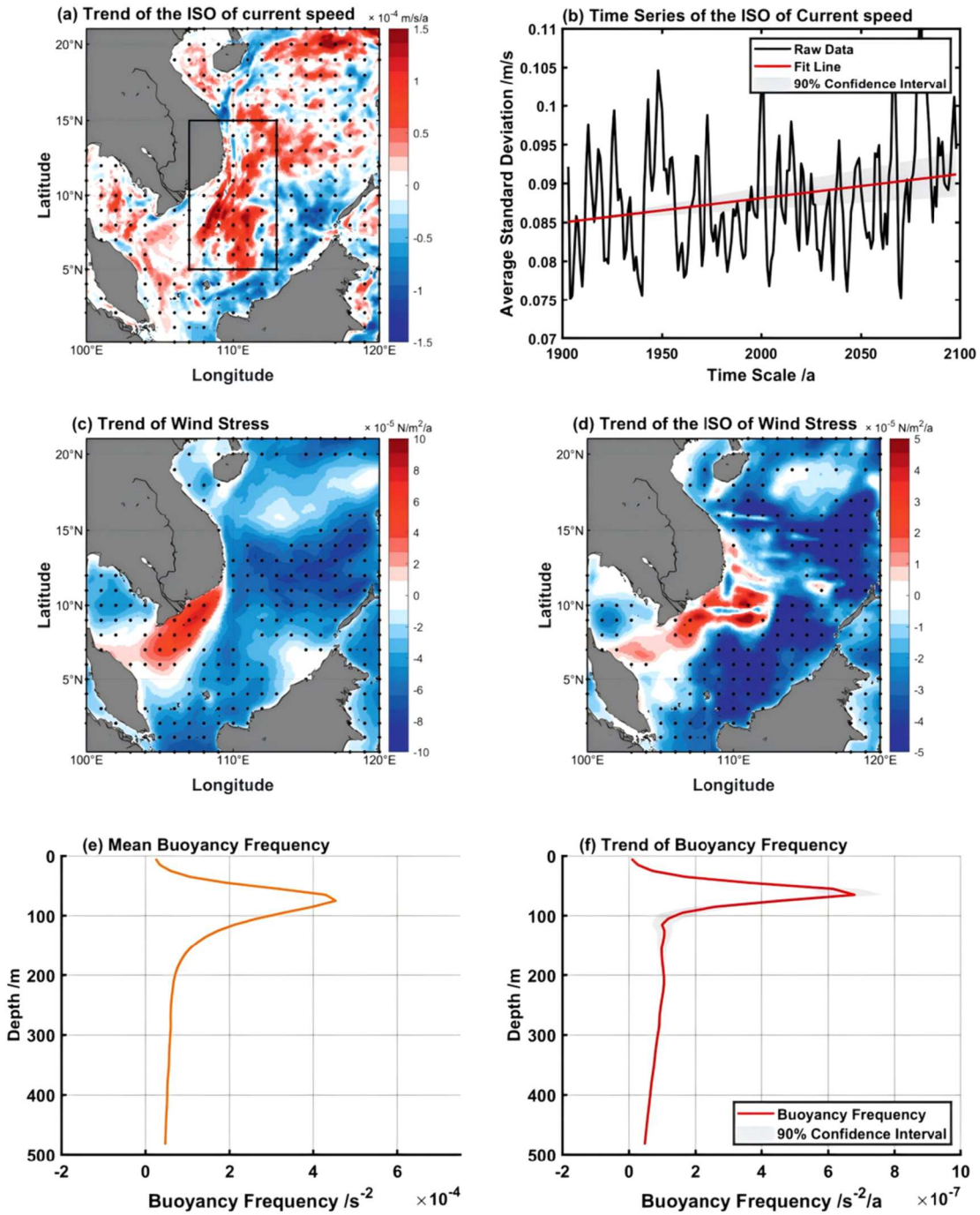

Figure 2. (a) Space distribution of linear trend of the *ISO_cur*, with a black rectangle representing the WBC. (b) Time series of *ISO_cur* in the black box in figure 2(a). (c) Space distribution of linear trend of wind stress. (d) Linear trend of ISO of wind stress. (e) Mean buoyancy frequency in the upper-500 m ocean for representing stratification. (f) Linear trend of buoyancy frequency. Here, the time range is 1901–2100, and the black dots in a, c, d and the shading in b, f both represent 90% confidence.

speed oscillations (Wang *et al* 2013; figure S2), indicating the CESM model is suitable for evaluating the long-term trend of ISO in upper-layer circulation.

3.2. Trends of the ISO of the current speed, wind and stratification

The spatial distribution of the linear trend of *ISO_cur* is shown in figure 2(a), in which *ISO_cur* depicts a robust increasing trend within 5°N–15°N, 107°E–113°E. It is noteworthy that the positive trend is mainly located within the strong current regions (figure 1(c)), indicating that the intensity of WBC is more likely to influence ISO intensity (Hu *et al* 2024). During 1901–2100, the WBC in the SCS exhibits a 7.87% enhanced trend of the ISO (figure 2(b)), with an increment of $3.12 \pm 1.47 \times 10^{-5}$ m·s^{-1} per year (3.12 is increasing rate of ISO generated by the regress function in MATLAB, while 1.47 is 90% t-test confidence interval radius).

In order to analyze the underlying mechanism of the intensifying *ISO_cur*, we further calculate the trends of wind stress and its ISO. Figure 2(c) indicates that the basin-scale wind stress weakens by about 0.014 $N{\cdot}m^{-2}$, equivalent to 10% of its climatology mean. The weakening wind stress leads to a decreasing current speed, restraining the ISO intensity through a weaker instability. To the south of Vietnam, sea surface wind stress shows a regional intensifying trend (figure 2(c)), however, these positive values are located to the west of the strong current region where *ISO_cur* depicts significant increasing trend (figure 2(a)). This mismatch in spatial distribution indicates the regional surface wind enhancement might not be the key reason for the positive trend in *ISO_cur*. The trend of the wind stress ISO demonstrates a similar spatial distribution with wind stress mean state, with an 18% basin scale weakening trend (figure 2(d)), suggesting a reduced external forcing for the *ISO_cur* (Hu *et al* 2024). Based on the discussions above, the weakening wind stress and its ISO may lead to a weaker upper-layer circulation oscillation; therefore, we further investigate the oceanic stratification in SCS under global warming. According to previous studies (Li *et al* 2020, Peng *et al* 2022), the intensity of stratification is evaluated by square of buoyancy frequency (N^2), which is defined as follows:

$$N^2 = -\frac{g}{\rho_0}\frac{d\rho}{dz}, \tag{8}$$

where $g = 9.8\ m{\cdot}s^{-1}$, ρ_0 is the background seawater density and $d\rho/dz$ is the vertical density gradient. Figure 2(e) denotes the buoyancy frequency in the upper 500 m of the whole SCS basin. It's found that the maximum N^2 reaches $4.53 \times 10^{-4}\ s^{-2}$ at 75-meter depth, below which and the stratification weakens with increasing depth (Lan *et al* 2006). The trend of average upper-layer buoyancy frequency shows a 24% strengthening in the 200-year period (figure 2(f)). The maximum N^2 increasing rate is located at 65-meter depth, with a value of $6.79 \times 10^{-7}\ s^{-2}$ per year, indicating a significant (~10%) uplift of the thermocline depth. This enhanced stratification, primarily driven by global warming, prevents the kinetic energy from transporting downward (Pedlosky 1987, Sun *et al* 2013), therefore enhancing the upper-layer circulation, and amplifying the upper-layer instabilities. The increase of upper-layer instabilities enhances the possibility of mean flow to vortex kinetic energy with a period of 20–90 days in the off-shore region of winter WBC (Lin *et al* 2015, Yao *et al* 2017, Feng *et al* 2017, Peng *et al* 2022, Zhu *et al* 2024, Yang *et al* 2025). Consequently, the intensification of the *ISO_cur* in the SCS is likely to be primarily driven by the strengthening stratification of the upper-ocean.

3.3. The intraseasonal impact of wind and stratification

To further consolidate the role of surface wind and oceanic stratification in affecting the intensification of the *ISO_cur* in the SCS, four idealized high-resolution experiments based on the QG model introduced in section 2.1.3 are conducted (table S1), with robustness confirmed via sensitivity analysis (tables S3, S4; figure S3). In the first experiment, namely Before-Warming-Run, the wind stress intensity (τ_0) is set to be $4.5 \times 10^{-6}\ N{\cdot}m^{-2}$ while the amplitude of wind stress ISO (k) is set to be 9.900. Following the previous studies (Yang *et al* 2017, Sun and Lan 2023), parameters representing the intensity of stratification, that is, the upper-layer thickness H_1 and reduced gravity g', are set to be 220 m and $0.03\ m{\cdot}s^{-2}$, respectively (table S1). In the second experiment (called After-Warming-Run), τ_0 and k are set to be $4.0 \times 10^{-6}\ N{\cdot}m^{-2}$ and 8.625, representing 10% and 13% weakening rate compared with Before-Warming-Run, which is the same as the weakening rate in CESM. In addition, the reduced gravity g' and upper-layer thickness H_2 are $0.037\ m{\cdot}s^{-2}$ and 200 m, denoting a 23% increase of stratification and 10% uplift of the thermocline, both comparable with the changing rate in CESM data. The third experiment (Wind-Weakening-Run) isolates the effect of wind field change. It uses the τ_0 and k in After-Warming-Run combined with H_1 and g' in Before-Warming-Run. Similarly, the last experiment (Stratification-Strengthening-Run) uses enhanced stratification but remains wind field unchanged to highlight the impact of stratification on the ISO of upper-layer circulation. Detailed setting is available in table S1.

Figure 3(a) compares the WBC transport (left panel) as well as *ISO_cur* (right panel) in CESM and QG model. Before global warming, the volume transport of WBC in CESM reaches 9.64 Sv (calculated in the black rectangle in figure 1(c) during 1901–1930). In comparison, the WBC in Before-Warming-Run transports 9.24 Sv water mass southward (dashed yellow rectangle in figure 3(c)), showing a great consistency with the CESM data. In addition, the ISO of WBC in CESM reaches $0.089\ m{\cdot}s^{-1}$ (calculated in the black rectangle in figure 2(a) during 1901–1930), while the WBC in Before-Warming-Run reaches $0.097\ m{\cdot}s^{-1}$ (solid yellow rectangle in figure 3(c)). Therefore, the QG model reasonably reproduces the dynamics of the SCS upper-layer circulation and the model parameters in table S1 are suitable. After global warming, the volume transport of WBC in CESM reduces to 9.52 Sv (calculated in the black rectangle in figure 1(c) during 2071–2100). In comparison, the WBC in After-Warming-Run transports 8.86 Sv water mass southward (dashed yellow rectangle in figure 3(d)), showing a great consistency with the CESM data. In addition, the ISO of WBC in CESM reaches $0.096\ m{\cdot}s^{-1}$ (calculated in the black rectangle in figure 2(a) during 2071–2100), while the WBC in After-Warming-Run reaches $0.101\ m{\cdot}s^{-1}$ (solid yellow rectangle in figure 3(d)). Therefore, the QG model reasonably

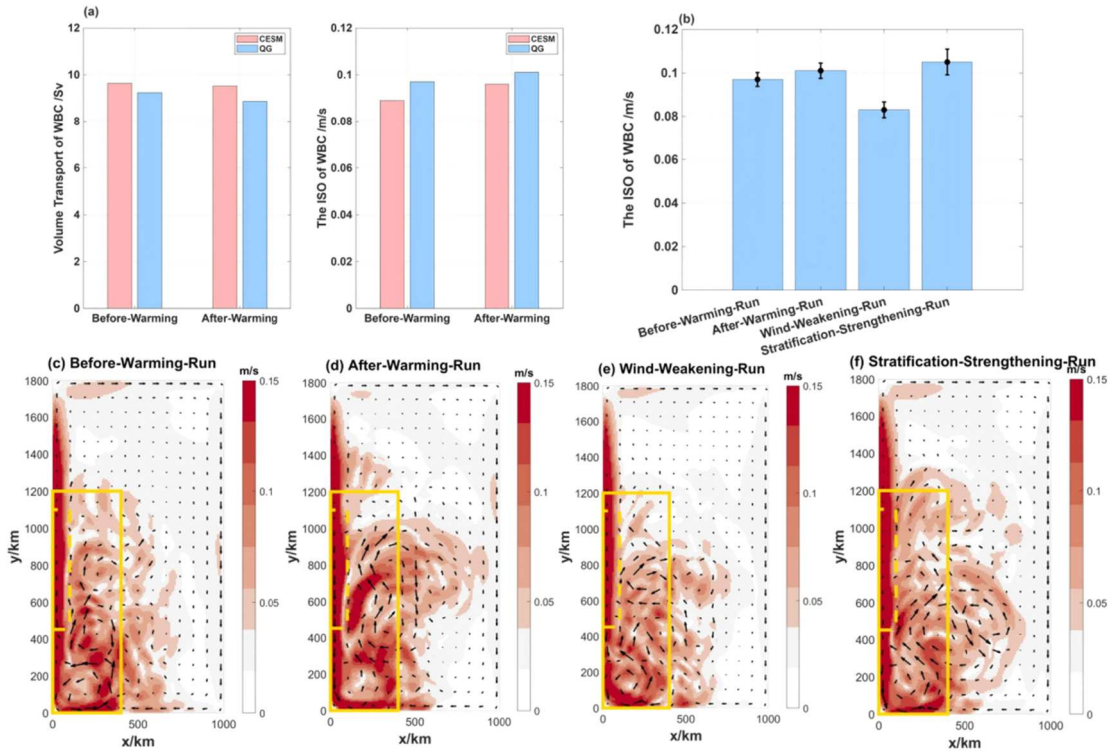

Figure 3. (a) The comparison between CESM and QG, using volume transport and ISO of WBC as criteria. (b) ISO of the WBC under four states (c-f) controlled by QG model, with error bars of 95% t-test. (c) ISO of the current speed in Before-Warming-Run. (d) ISO of the current speed in After-Warming-Run. (e) ISO of the current speed in Wind-Weakening-Run. (f) ISO of the current speed in Stratification-Strengthening-Run. The solid yellow rectangle in c~f is the calculated space of the ISO of WBC, and the dashed rectangle is the calculated space of volume transport.

reproduces the variation of the SCS upper-layer circulation under global warming by revising wind and stratification, proving the significant effect of wind and stratification.

After confirming the capacity of the QG model in reproducing the evolution of *ISO_cur* under global warming, the Wind-Weakening-Run and the Stratification-Strengthening-Run are conducted. The *ISO_cur* in Wind-Weakening-Run reduces to 0.083 m·s^{-1}, indicating a 14.43% weakening compared with the status before warming (figures 3(b), (c) and (e); table S2), demonstrating that weakened wind fields result in a weaker ISO of WBC (Hu *et al* 2024). If we keep the wind field unchanged and only modify the stratification to the state after warming, the *ISO_cur* increases to 0.105 m·s^{-1} and has a 8.25% strengthening (figures 3(b), (c) and (f); table S2), demonstrating that strengthening stratification favors an enhanced ISO of WBC (Peng *et al* 2022, Yang *et al* 2025). Consequently, the intensification of the ISO of the WBC in the SCS is primarily driven by the strengthening stratification of the upper-ocean, and the wind forcing has a secondary role.

4. Potential implications of ISO intensification

The intensification of the ISO of current speed not only reflects the evolution of the SCS current system under global warming, it may also affect the surrounding ocean environment and overlying atmosphere through the ISO of SST and surface heat flux (SHF; Duvel and Vialard 2007). Based on CESM data, we explore the linear trends of the ISO of SST and SHF during 1901–2100 (figure 4; equation (7)). It's found that the ISO of SST depicts a similar distribution with that of current speed (figures 2(a) and 4(a)), with an increasing rate about $9.56 \pm 7.20 \times 10^{-5}$ °C per year in the WBC region. Further analysis shows that the ISO of SST and current speed are highly related, with a correlation coefficient reaching 0.60 in the WBC region over the 200-year period (figure 4(b)). This relationship suggests that the intensification of the ISO of current speed may influence the SST by heat transport (Johns *et al* 2011, Parfitt *et al* 2017, Sen Gupta *et al* 2021, Cai *et al* 2023). The enhanced SST oscillation induces possibility of larger intensity and frequency of marine heatwaves in SCS (Cai and Tan 2024, Meng *et al* 2024), which may disturb marine ecosystems and then reduce biodiversity (Wernberg *et al* 2016, Hughes *et al* 2017, Joyce *et al* 2024, Meng *et al* 2024).

In addition, the ISO of SHF also shows an intensifying pattern in the extension region of winter WBC of SCS (figures 4(c), (d)). Correlation analysis implies that SHF and SST are negatively correlated in the

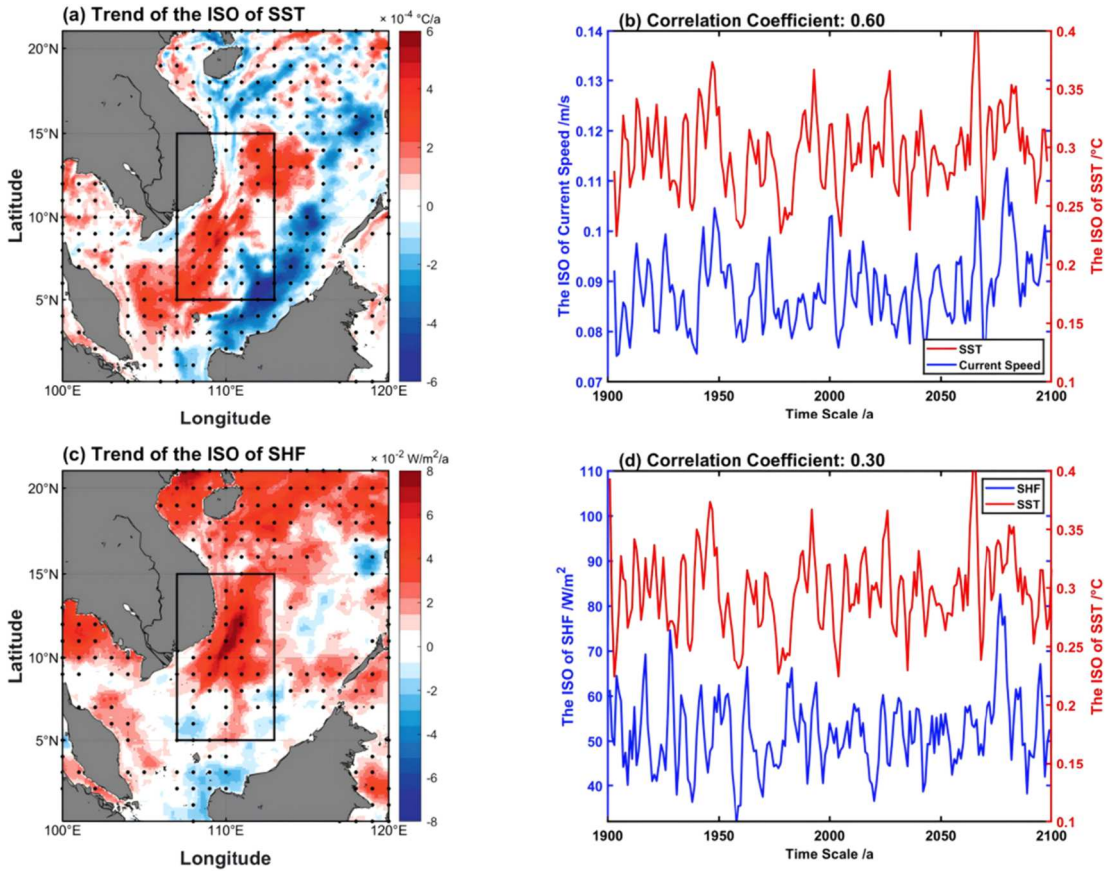

Figure 4. (a) Space distribution of linear trend of ISO of SST. (b) The time series of ISO of SST and current speed in the WBC region, with correlation coefficient about 0.60. (c) Space distribution of linear trend of ISO of SHF. (d) The time series of ISO of SHF and SST in the WBC region, with correlation coefficient about 0.30. The black rectangles in a and c represent the WBC, and the black dots represent 90% confidence.

intraseasonal timescale (figure S1, negative SHF represents ocean releases heat into the atmosphere), suggesting the increasing ISO of SST might enlarge ocean heat release. Therefore, *ISO_cur* may also partly affect the local atmospheric processes and regional climate through SST oscillations under global warming (Liu *et al* 2004).

5. Summary

Based on both CESM and QG model, the trend of the ISO of upper-layer circulation in the winter of SCS is studied. The major results of this study are summarized as follows:

1. In the winter SCS, the ISO of current speed shows a 7.87% strengthening trend in the WBC region during 1901–2100.
2. The sea surface wind stress and its ISO weaken by 10% and 18%, respectively. By comparison, a 24% strengthening trend in the stratification is considered and demonstrated to insert a significant impact on the intensification of the ISO of WBC by QG experiments.
3. Correlation analysis shows that the ISO of current speed may affect the ISO of SST through oceanic heat transport, which may lead to enhanced intensity and frequency of marine heatwaves in the SCS. In addition, the enhanced ISO of SST may further influence the SHF in the region of WBC and then alters local atmospheric processes and regional climate in a warming climate.

Data availability statement

The HR CESM simulations can be accessed from https://ihesp.github.io/archive/products/ds_archive/Sunway_Runs.html. The surface geostrophic speed products provided by the ECCO2 can be downloaded at https://data.nas.nasa.gov/ecco/. The data that support the findings of this study are openly available at the URL/DOI.

Acknowledgments

This work was supported by the National Key Research and Development Program of China (2022YFC3104801), National Natural Science Foundation of China (42422601, 42176006) and Laoshan Laboratory Science and Technology Innovation Project (LSKJ202202503). Computation for this work is supported by the Marine Big Data Center of Institute for Advanced Ocean Study of Ocean University of China and Laoshan Laboratory.

Conflict of interest statement

The authors declare no competing interests.

Ethical statements

This work does not involve live subjects (humans or animals).

Author contributions

Jingyao Cai
Formal analysis (equal), Writing – original draft (equal)

Mingkui Li
Writing – review & editing (equal)

Jinzhuo Cai 0000-0003-1455-1156*
Xin Ma
Writing – review & editing (equal)

Haiyuan Yang 0000-0002-9662-6993
Xingzhi Zhang
Writing – review & editing (equal)

Jingjie Yu 0000-0001-7707-1630
Writing – review & editing (equal)

Zhaohui Chen
Writing – review & editing (equal)

References

Berloff P, Hogg A M C and Dewar W 2007 The turbulent oscillator: a mechanism of low-frequency variability of the wind-driven ocean gyres *J. Phys. Oceanogr.* **37** 2363–86
Cai J, Yang H, Gan B, Wang H, Chen Z and Wu L 2023 Evolution of meridional heat transport by subtropical western boundary currents in a warming climate predicted by high-resolution models *J. Clim.* **36** 8007–25
Cai R and Tan H 2024 Progress on the evolutionary characteristics and climatic causes for warming and marine heatwaves in the Coastal China Seas *Chin. J. Atmos. Sci* **48** 121–46
Cao X, Wu R and Chen S 2017 Contrast of 10–20-day and 30–60-day intraseasonal SST propagation during summer and winter over the South China Sea and western North Pacific *Clim. Dyn.* **48** 1233–48
Chang P *et al* 2020 An unprecedented set of high-resolution Earth system simulations for understanding multiscale interactions in climate variability and change *J. Adv. Model. Earth Syst.* **12** e2020MS002226
Chu P, Edmonds N, Fan and C 1999 Dynamical mechanisms for the South China Sea seasonal circulation and thermohaline variabilities *J. Phys. Oceanogr.* **29** 2971–89
Dong M, Wu T, Wang Z and Zhang F 2009 Simulations of the tropical intraseasonal oscillation in the National Climate center's Atmospheric general model *Acta Meteorol. Sin.* **67** 912–22
Duvel J P and Vialard J 2007 Indo-pacific sea surface temperature perturbations associated with intraseasonal oscillations of tropical convection *J. Clim.* **20** 3056–82
Fang G *et al* 2012 A review on the South China Sea western boundary current *Acta Oceanol. Sin.* **31** 1–10
Fang W, Fang G, Shi P, Huang Q and Xie Q 2002 Seasonal structures of upper layer circulation in the southern South China Sea from *in situ* observations *J. Geophys. Res.* **107** 1–
Feng B, Liu H, Lin P and Wang Q 2017 Meso-scale eddy in the South China Sea simulated by an eddy-resolving ocean model *Acta Oceanol. Sin.* **36** 9–25
Ferrari R and Wunsch C 2009 Ocean circulation kinetic energy: reservoirs, sources, and sinks *Annu. Rev. Fluid Mech.* **41** 253–82

Gan J and Qu T 2008 Coastal jet separation and associated flow variability in the southwest South China Sea *Deep-Sea Res. Part I* **55** 1–19
Hu Z, Lyu K and Hu J 2024 Modulations of the South China Sea Ocean circulation by the summer monsoon intraseasonal oscillation inferred from satellite observations *Remote Sens.* **16** 1195
Hu J, Kawamura H, Hong H and Qi Y 2016 A review of research on the upwelling in the South China Sea *Rev. Geophys.* **54** 653–73
Hughes T P *et al* 2017 Global warming and recurrent mass bleaching of corals *Nature* **543** 373–7
Johns W E *et al* 2011 Continuous, array-based estimates of Atlantic Ocean heat transport at 26.5°N *J. Clim.* **24** 2429–49
Joyce P W S, Tong C B, Yip Y L and Falkenberg L J 2024 Marine heatwaves as drivers of biological and ecological change: implications of current research patterns and future opportunities *Mar. Biol.* **171** 1–13
Kang S, Wang X, Du J and Song Y 2022 Paleoclimates inform on a weakening and amplitude-reduced East Asian winter monsoon in the warming future *Geology* **50** 1224–8
Kelly P M and Jones P D 1996 Removal of the El Niño-Southern Oscillation signal from the gridded surface air temperature data set *J. Geophys. Res. Atmos.* **101** 19013–22
Lan J, Bao Y, Yu F and Sun S 2006 Seasonal changes of deep-water circulation and thermocline depth in the South China Sea *Adv. Mar. Sci. (in Chinese)* **24** 436–46
Li C and Qu X 1999 Large scale atmospheric circulation evolutions associated with summer monsoon onset in the South China Sea *Chin. J. Atmos. Sci.* **24** 1–14
Li G *et al* 2020 Increasing ocean stratification over the past half-century *Nat. Clim. Change* **10** 1116–23
Liu Z 1997 The influence of stratification on the inertial recirculation *J. Phys. Oceanogr.* **27** 926–40
Liu Q, Jiang X, Xie S-P and Liu W T 2004 A gap in the Indo-Pacific warm pool over the South China Sea in boreal winter: dynamics and seasonal interannual variability *J. Geophys. Res. Oceans* **109** C07012
Liu X, Liang C and Lin F 2023 Cases study of intraseasonal variability of velocity happened in spring in the northern South China Sea *Acta Oceanol. Sin.* **45** 1–12
Lin X, Dong C, Chen D, Liu Y, Yang J, Zou B and Guan Y 2015 Three-dimensional properties of mesoscale eddies in the South China Sea based on eddy-resolving model output *Deep Sea Res. Part I* **99** 46–64
Meng L *et al* 2024 Characteristics and mechanism of winter marine heatwaves in the cold tongue region of the South China Sea *Front. Mar. Sci.* **11** 1362805
Parfitt R, Czaja A and Kwon Y-O 2017 The impact of SST resolution change in the ERA-Interim reanalysis on wintertime Gulf Stream frontal air-sea interaction *Geophys. Res. Lett.* **44** 3246–54
Pedlosky J 1987 *Geophys. Fluid Dyn.* 2nd edn (Springer)
Peng Q, Liang X, Dong Y and Liu Y 2022 Surface warming–induced global acceleration of upper ocean currents *Sci. Adv.* **8** eabj8394
Qiu B and Chen S 2005 Variability of the Kuroshio Extension jet, recirculation gyre, and mesoscale eddies on decadal time scales *J. Phys. Oceanogr.* **35** 2090–103
Shang Y, Liu P and Wu S 2023 Responses of the Pacific and Atlantic decadal variabilities under global warming by using CMIP6 models *Ocean Dyn.* **74** 64–75
Shaw P T and Fu L L 1999 Sea surface height variations in the South China Sea from satellite altimetry *Oceanol. Acta* **22** 1–17
Sen Gupta A *et al* 2021 Future changes to the upper ocean western boundary currents across two generations of climate models *Sci. Rep.* **11** 9538
Sun Y and Lan J 2023 Interannual migration of the summertime eastward jet in the South China Sea associated with the upper layer thickness distribution *J. Geophys. Res. Oceans* **128** e2023JC019920
Sun S, Wu L and Qiu B 2013 Response of the inertial recirculation to intensified stratification in a two-layer quasigeostrophic ocean circulation model *J. Phys. Oceanogr.* **43** 1254–69
Taylor K E, Stouffer R J and Meehl G A 2012 An overview of CMIP5 and the experiment design *Bull. Am. Meteorol. Soc.* **93** 485–98
von Schuckmann K *et al* 2020 Heat stored in the Earth system: where does the energy go? *Earth Syst. Sci. Data* **12** 2013–41
Wan X, Liu Z, Shen B, Lin X and Wu D 2014 Introduction to the community earth system model and application to high performance computing *Adv. Earth Sci.* **29** 482–91
Wang S *et al* 2024 A more quiescent deep ocean under global warming *Nat. Clim. Change* **14** 961–7
Wang D, Liu Q, Huang R X, Du Y and Qu T 2006 Interannual variability of the South China Sea associated with El Niño *J. Geophys. Res. Oceans* **111** C03023
Wang D *et al* 2013 Progress of regional oceanography study associated with western boundary current in the South China Sea *Chin. Sci. Bull.* **58** 1205–15
Wang H and He S 2012 Weakening relationship between East Asian winter monsoon and ENSO after mid-1970s *Chin. Sci. Bull.* **57** 3535–40
Wang Q *et al* 2020 Intraseasonal variability of cross-slope flow in the northern South China Sea *J. Phys. Oceanogr.* **50** 2071–84
Wernberg T *et al* 2016 Climate-driven regime shift of a temperate marine ecosystem *Science* **353** 169–72
Wu C-R, Shaw P-T and Chao S-Y 1998 Seasonal and interannual variations in the velocity field of the South China Sea *J. Oceanogr.* **54** 361–72
Xu X and Wang X 2024 The QG limit of the rotating thermal shallow water equations *J. Differ. Equ.* **401** 1–29
Xu X, Qiu Z and Chen H 1982 The general description of the horizontal circulation in the South China Sea *Proc. 1980 Symp. Hydrometeorol. Chin. Soc. Oceanol. Limnol. (Beijing)* (Science Press) 137–45
Yang H J and Liu Q Y 1998 A summary on ocean circulation study of the South China Sea *Adv. Earth Sci.* **13** 364–8
Yang H-Y *et al* 2025 Onshore intensification of subtropical western boundary currents in a warming climate *Nat. Clim. Change* **15** 301–307
Yang H, Wu L, Sun S and Chen Z 2017 Selective response of the South China Sea circulation to summer monsoon *J. Phys. Oceanogr.* **47** 1555–68
Yang H Y, Wu L X, Sun S T and Chen Z H 2015 Low-frequency variability of monsoon-driven circulation with application to the South China Sea *J. Phys. Oceanogr.* **45** 1632–50
Yao J-L, Li H, Liu Q-Y, Wang Q, Xiao F-A, Wang D-X and Zu T-T 2017 Energy diagnostic of the mesoscale processes loaded by the South China Sea throughflow *Oceanol. Limnol. Sin.* **48** 1257–68
Zhou W and Chan J C L 2005 Intraseasonal oscillations and the South China Sea summer monsoon onset *Int. J. Climatol.* **25** 1585–609
Zhuang W *et al* 2010 Intraseasonal variability in sea surface height over the South China Sea *J. Geophys. Res.* **115** C04010
Zhu L, Atoufi A, Lefauve A, Kerswell R R and Linden P F 2024 Long-wave instabilities of sloping stratified exchange flows *J. Fluid Mech.* **983** A12